Research Article | Vol. 12, No. 7 / 1 Jul 2022 / Optical Materials Express 2453
Optical Materials EXPRESS

Tunable infrared high absorbing polarization independent niobium nitride plasmonic perfect absorber nanowire photodetectors

PHILIPP KARL,[1,*] SANDRA MENNLE,[1] MONIKA UBL,[1] MARIO HENTSCHEL,[1] PHILIPP FLAD,[1] JING-WEI YANG,[2,3] TZU-YU PENG,[2,3] YU-JUNG LU,[2,3] AND HARALD GIESSEN[1]

[1]4th Physics Institute and Research Center SCoPE, University of Stuttgart, Pfaffenwaldring 57, 70569 Stuttgart, Germany
[2]Research Center for Applied Sciences, Academia Sinica, Taipei 11529, Taiwan
[3]Department of Physics, National Taiwan University, Taipei 10617, Taiwan
[*]philipp.karl@pi4.uni-stuttgart.de

Abstract: The recent development of photon-based technologies such as quantum cryptography and quantum computing requires high fidelity and fast photodetectors, as well as the ability to detect single photons. One possibility to achieve these goals are superconducting nanowire single photon detectors, utilizing the superconducting-to-normal conducting phase transition. To achieve the required high efficiency, we use resonant plasmonic perfect absorber effects, reaching over 90% polarization-independent absorbance at our target wavelength of 1140 nm. Moreover, the target wavelength can be easily tuned by adjusting the geometry of our detectors. Furthermore, the high absorbance is maintained at oblique incidence, due to the plasmonic perfect absorber principle, and small active areas can be achieved by the high resonant absorption cross-section of plasmonic resonances. We fabricated different tunable, polarization independent plasmonic perfect absorber superconducting nanowire photodetectors and proved their high absorbance and polarization independent response in the wavelength regime around 1140 nm.

1. Introduction

Highly efficient, precise and fast single photon detectors are required for quantum information technologies such as quantum computing [1,2] and quantum key distribution [3], to ensure a secure form of communication. For these reasons, single photon detectors become an interesting and exiting field of research. The necessary requirements can be fulfilled by so-called Superconducting Nanowire Single Photo Detectors [4–6] (SNSPDs). Creating small and efficient photodetectors is challenging, due to the tradeoff between short recovery times, caused by small active-areas, and high detection efficiencies accomplished by large active-areas [7]. This can be tackled by utilizing plasmonic resonances with their large resonant absorption cross section.

The general properties of SNSPDs are determined by their material and design, which leads to a great variety of different detector types made from various superconducting materials such as niobium titanium nitride [8–10], tungsten silicide [11], and niobium nitride (NbN) [12–14], featuring differing designs such as optical cavities [15], waveguides [16], and plasmonic nanostructures [5,17,18].

A typical design is the meander structure. This design is usually sensitive to the polarization of the incident light, hence the detection efficiency varies for different polarized photons [19,20]. Depending on the application for which the detectors are intended, this is an undesired effect. For example, when fiber coupling with normal single-mode fibers, the polarization is not preserved, therefore a high detection efficiency in every polarization direction is important. There are several

#458242 https://doi.org/10.1364/OME.458242
Journal © 2022 Received 10 Mar 2022; revised 5 May 2022; accepted 7 May 2022; published 7 Jun 2022

Optical Materials EXPRESS

approaches to achieve this goal, such as fractal nanostructures [21], double-layer systems [22], and spiral nanostructures [23].

Plasmonic nanostructures and their localized surface plasmons [24] are already used in a variety of different applications [25,26] and additionally, plasmonic enhancement is already used for other types of infrared photodetectors [27–29]. Depending on their design they offer polarization-dependent and polarization-independent responses. Moreover, they can provide small and fast detectors due to the high resonant absorption cross section. This can be enhanced even further by utilizing the so-called plasmonic perfect absorber principle [30,31], leading to absorption of up to 100% and strong incident angle independence [32,33]. These type of plasmonic perfect absorber sensors are already used for other sensing technologies [34].

In this work we present two different tunable polarization-independent plasmonic perfect absorber superconducting nanowire photodetector designs and prove their high absorbance, tunability, and polarization independent response in the near infrared spectral range.

2. Sample fabrication

To ensure the best possible optical properties for our NbN detectors we need to precisely define our structures. This high quality, precision, and control can be obtained by using electron beam lithography (EBL) combined with plasma etching techniques. Figure 1 depicts a schematic sketch of this fabrication process.

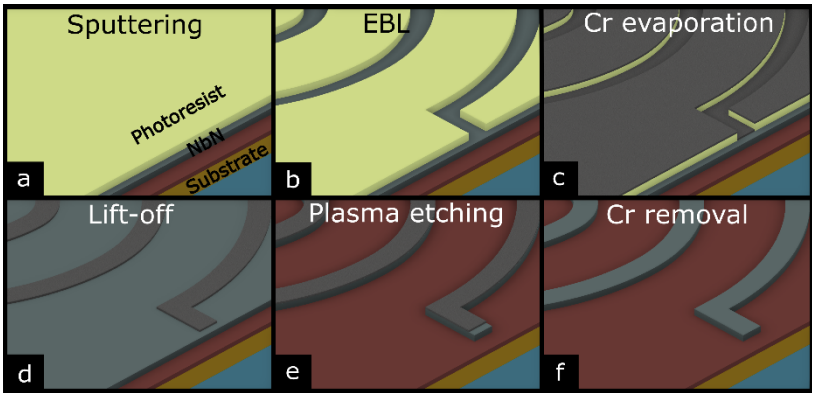

Fig. 1. Fabrication of the nanostructures: (a) High resolution photoresist is spin-coated on top of the sputtered NbN layer. (b) An inverse pattern of the desired nanostructure is created with electron beam lithography. (c) A Cr layer is evaporated on top of the structured photoresist. (d) By removing the photoresist only the Cr etching mask of the desired structure is left. (e) Plasma etching creates the NbN nanostructure. (f) Removing the Cr etching mask.

The sample consists of a glass substrate, followed by a 5 nm thick titanium sticking layer and the perfect absorber substrate which consist of two parts, a 120 nm thick gold film and a 100 nm thick aluminum oxide (Al_2O_3) dielectric spacer. To obtain a clean and smooth surface the metallic parts are evaporated via electron gun and the Al_2O_3 via atomic layer deposition (R-200 Advanced, Picosun).

The 20 nm thick plasmonic NbN film was sputter-deposited onto the prepared perfect absorber substrate using radio-frequency magnetron sputtering, with a NbN target, a deposition temperature of 800°C, a chamber pressure of $< 6 \times 10^{-8}$ torr, a nitrogen/argon flow rate ratio of 1/24 and a power of 120 W. We note that the properties of the NbN film can be varied with different parameters [35,36]. In the end, the chamber is vented with nitrogen at room temperature. These growth parameters ensure the highest possible critical temperature.

Optical Materials EXPRESS

Afterwards a high resolution positive photoresist (AR-P 6200.04 CSAR62, Allresist), and Espacer (Showa Denko) is spin-coated on top, as shown in Fig. 1(a). To create an inverse pattern of our desired nanostructure we expose the photoresist via electron beam patterning (eLine Plus, Raith), as depicted in Fig. 1(b). Figure 1(c) and (d) illustrate the evaporation and lift-off of the 50 nm thick Chromium (Cr) etching mask. First we cover the entire film with Cr, which is evaporated via electron gun evaporation and remove the undesired Cr with a lift-off process, using a n-ethyl-2-pyrrolidon based remover (Allresist), leaving the finished Cr etching mask on the NbN film. The uncovered NbN is removed via plasma etching, see Fig. 1(e). The last step is to remove the Cr via a commercial Cr remover, shown in Fig. 1(f). This process yields high-quality nanostructures. Moreover, it allows us to simply change the design and geometry of our detectors and therefore tune the plasmonic resonance and the absorption of our detectors to desired wavelengths.

3. Detector design, absorption, and response

3.1. Plasmonic perfect absorber

Figure 2 depicts the working principle and substrate design of the NbN plasmonic perfect absorber samples.

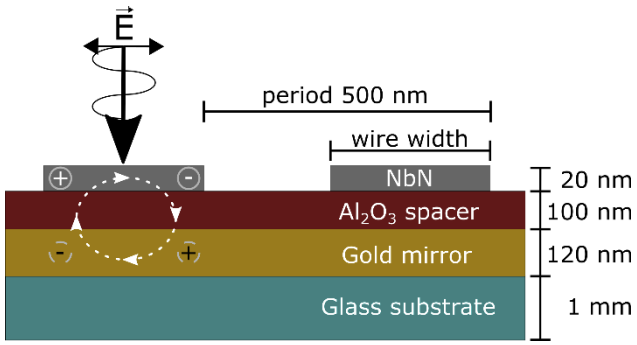

Fig. 2. Working principle and substrate design of the NbN plasmonic perfect absorber. Left: Representation of the plasmonic perfect absorber principle. The incoming light leads to a plasmon oscillation in the NbN wire on the top. Thus, an antiphase oscillating mirror plasmon is created in the gold mirror below. Their interaction creates a circular current and a magnetic response. Right: Schematic structure of our NbN perfect absorber samples.

The plasmonic perfect absorber principle enables us to reach high absorbance at our desired wavelengths. There are two different ways to explain this phenomenon. The first explanation is shown in Fig. 2 on the left side. When light, which is polarized perpendicular to the NbN wire, hits the nanostructure it excites a localized surface plasmon. Due to this oscillating plasmon an antiphase oscillating mirror plasmon is generated in the gold mirror below. The interaction between these two plasmons initiates a circular current, resulting in a magnetic response, which interacts with the magnetic field of the incoming light.

The second method is a mathematical model, where we can describe the sample as a medium with the electric permittivity $\varepsilon(\lambda)$ und the magnetic permeability $\mu(\lambda)$. By impedance matching between the surface impedance of our structure $Z_s = (\mu/\varepsilon)^{1/2}$ and the vacuum impedance $Z_v = 1$, we can suppress the reflectance $R = |(Z_v - Z_s)/(Z_v + Z_s)|^2$ of the sample. Impedance matching is optimized by the geometric parameters such as periodicity, spacer thickness, and wire width. To find the starting parameter for these optimizations we carry out electromagnetic simulations, using an in-house implementation of the Fourier modal method, utilizing a scattering matrix approach and 255 plane waves [37,38]. The simulations are performed with air as upper material

Optical Materials EXPRESS

and the perfect absorber layer as substrate. In addition, to reach the 100% absorbance, we need to block the transmission (T). In the infrared spectral range the incident light is blocked due to the thick gold mirror. The combination between suppressed reflection and blocked transmission leads to an absorbance A = 1 – R – T = 1 in the optimized spectral range [18,31,32].

Our samples are optimized for the near infrared spectral range around 1140 nm. The resulting geometric parameters are depicted in Fig. 2, on the right side. The periodicity is 500 nm, the Al_2O_3 dielectric spacer has a thickness of 100 nm, and the thickness of the gold mirror is 120 nm. The plasmonic structures consist of 20 nm thick NbN with variable wire widths to tune their fundamental dipole resonance [39] and thus the maximum absorbance to our desired wavelengths.

3.2. Polarization dependence and absorption

In Fig. 3 we point out the polarization sensitivity for the incident light of three different detector structures.

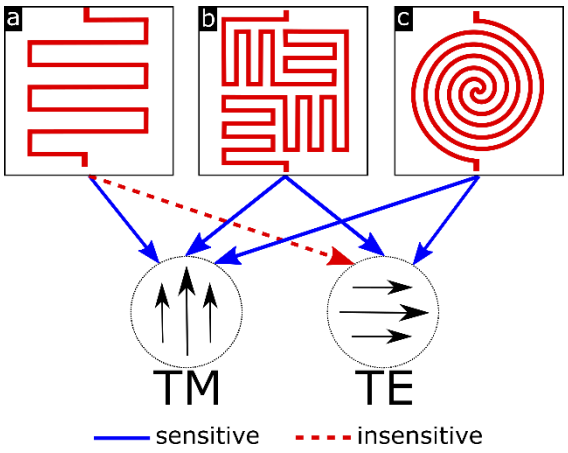

Fig. 3. Schematic drawing of different detector designs and their plasmonic polarization dependencies for TM and TE polarization.

The detector structure, shown in Fig. 3(a), is a typical grid-like meander used for a variety of detectors. In our case this structure shows a strong polarization dependence, due to the fact that plasmons are only excited when the polarization of the incoming light is perpendicular to the NbN wires [18]. Therefore, the perfect absorber principle can be applied for the TM polarization, and for the TE polarization only the intrinsic absorbance of the material is causing a detector response.

The structure, depicted in Fig. 3(b), is a combination of perpendicularly arranged meander-like structures. Thanks to this arrangement it covers TM as well as TE polarizations. This advantage comes with the drawback of halving the active-area for each polarization, due to the fact that only half of the structure can efficiently absorb one polarization, leading to a slight decrease in the absorbance and the detection efficiency.

In Fig. 3(c) a circular detector is shown. From the middle of this structure, the incoming light sees a steady plasmonic lattice in every direction, leading to polarization independence and high absorption for both polarizations. Thanks to the strong angle of incidence independence of the plasmonic perfect absorber substrate [18,32] the incident light can be focused in the middle without losing detection efficiency. One way to achieve this is fiber coupling with high-NA micro-optics at the end of optical fibers [40–42]. Moreover, this enables extremely small active areas, leading to small kinetic inductances and short recovery times. A typical optical fiber, for the infrared spectral range, has a core diameter of 6–8 µm, leading to minimum useful active

Optical Materials EXPRESS

areas of 6×6 μm^2. With precise 3D printing application and high-NA micro-optics, even 3×3 μm^2 active areas could be achieved [40], with our detectors. Decreasing the minimum active area by at least a factor of 4. Taking this into account and comparing the recovery time with literature, we expect recovery times in the lower nanosecond regime [43,44].

In Fig. 4 we present scanning electron microscope (SEM) images of the two finished polarization-independent detectors and their absorption spectra. In addition, we demonstrate the wavelength tunability of the absorbance by presenting structures of the same type, but with different wire widths. Figure 4(a) shows the SEM image of the meander-type and Fig. 4(b) depicts the SEM image of the circular-type detector, consisting of a 20 nm thick NbN detector structure, with a wire width of 215 nm, a period of 500 nm, and an active-area of 30×30 μm^2.

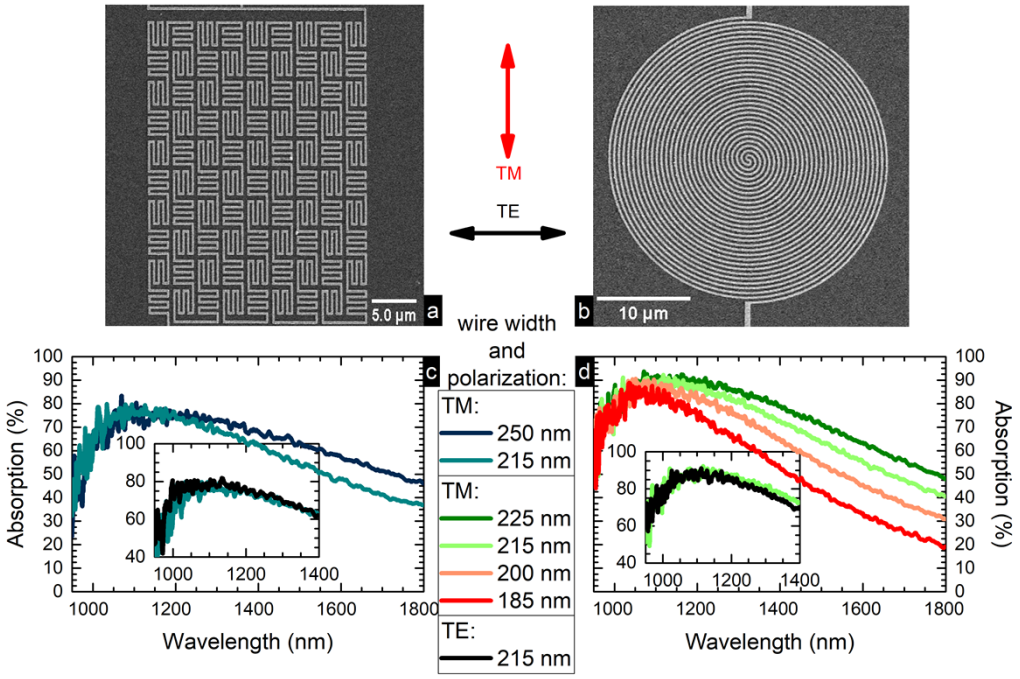

Fig. 4. (a) SEM image of the meander-type, polarization independent, 20 nm thick NbN detector structure, with a wire width of 215 nm and a period of 500 nm. The different horizontal and vertical wires react to different polarizations. (b) SEM image of the circular polarization independent, 20 nm thick NbN detector structure, with a wire width of 215 nm and a period of 500 nm. The center of the structure forms a symmetrical grid in all directions. (c) Absorption spectra of the 20 nm thick NbN meander-type detector, with a period of 500 nm, different wire thicknesses and an active area of 30×30 μm^2. The inset depicts the comparison of different polarizations. (d) Absorption spectra of the 20 nm thick circular NbN detector, with a period of 500 nm, different wire thicknesses and an active area of 30×30 μm^2. The inset depicts the comparison of different polarizations.

To investigate the absorption behavior of the different structures we have measured the reflectance with a Fourier-transform infrared spectroscopy spectrometer (Bruker Vertex 80 microscope Hyperion 3000) and calculated the absorbance with $A = 1 - R - T$, with $T = 0$. Figure 4(c) plots the absorption spectra of the 20 nm thick NbN meander-type detector, with a period of 500 nm, different wire thicknesses, and an active-area of 30×30 μm^2. The absorption for this design reaches over 80% at the desired wavelength over a broad spectral range. For wider wire widths the maximum shifts red and the absorption becomes broader, due to the larger

Optical Materials EXPRESS

dipole moments of the electron oscillations. The inset confirms the polarization independence. Figure 4(d) depicts the absorption spectra of the 20 nm thick circular NbN detector, with a period of 500 nm, different wire thicknesses, and an active area of 30×30 μm^2. The absorption of this kind of detectors reaches over 90% for both polarizations, confirmed by the inset. The absorption shifts red for larger wire widths and becomes broader. In addition, by comparing the measured absorption with the absorption of other NbN SNSPDs, we would estimate a detection efficiency of over 75% [13,14]. Moreover, typical jitter times for SNSPDs made out of NbN are in the low picosecond regime and we estimate a similar behavior for our structures [12,14,45].

As discussed above, the absorption for the circular structures reach higher values when compared with the meander-type structure, due the almost complete symmetrical plasmonic lattice in every direction. There is still a small displacement in the center due to the fact that the structure has to form a continues wire. A perfect plasmonic lattice detector utilizing the plasmonic perfect absorber principle reaches absorption values of almost 100%, which we demonstrated and discussed in [18].

3.3. Detector response

To demonstrate the functionality of our detectors we expose them to an external light source under cryogenic conditions while applying a bias current and measure their detector response, manifested as a voltage drop.

A response is measured when a photon hits the superconducting nanostructure, leading to the creation of a so-called local hot spot caused by disturbance and heating of Cooper pairs. This results in an increase of the resistance, which will force the supercurrent to flow around the hot spot region. Exceeding the critical current density causes the structure to switch from its superconducting to its normal conducting state in the illuminated area.

Figure 5 depicts the normalized detector response for the three different structure designs, over various laser powers, represented as a voltage drop. The measurements were performed at 3.5 K with a laser light source (Topica ECDL Pro) at 1140 nm. To measure the detector response, we have used a four-point resistant measurement with a KEITHLY 2611B current source and a KEITHLY 2182A nanovoltmeter.

The responses represented in Fig. 5(a) and (b) confirm the functionality of our detectors. They show the same response for both polarizations, confirming polarization independence of the structures at 3.5 K. Moreover, no response above their critical temperature at 20 K is measurable, confirming the superconducting working principle of our detectors.

As reference, in Fig. 5(c) we show a structure which was characterized before [18]. This detector exhibits a strong polarization dependence, because plasmons are only exited in TM polarization. Due to the higher absorption in TM polarization the response of this light polarization is stronger. For powers above 80 μW the responses for both polarizations are indistinguishable due to the heating and subsequent loss of superconductivity induced by the high laser power.

Optical Materials EXPRESS

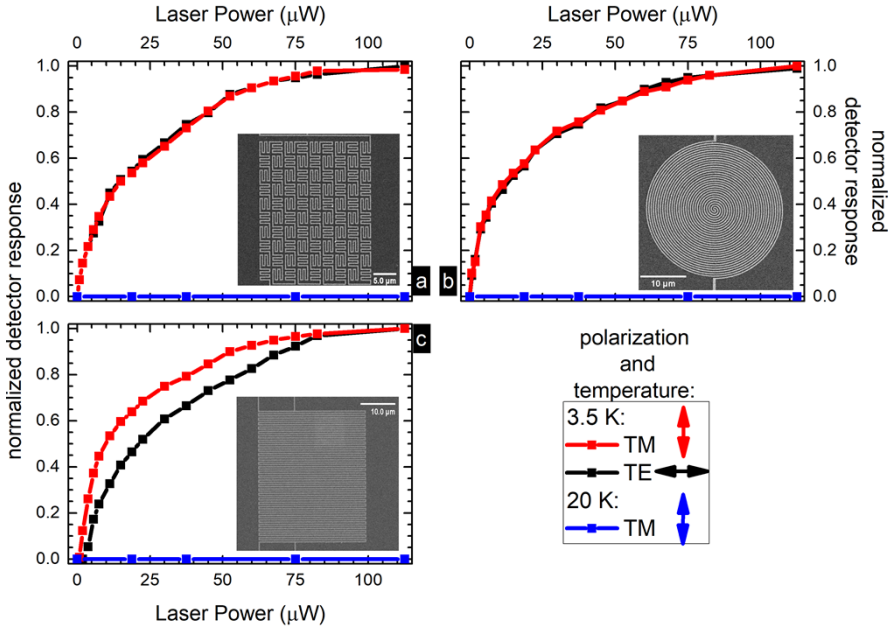

Fig. 5. Measured normalized detector response represented by a voltage drop for different polarizations at a wavelength of 1140 nm at 3.5 K and 20 K. (a) Measured detector response for the meander-type polarization-independent detector structure. No difference can be seen for the different polarizations. (b) Measured detector response for the circular polarization-independent detector structure. No difference can be observed for the different polarizations. (c) Measured detector response for the polarization-dependent detector structure. A clear difference can be identified for the different polarizations, because plasmons are only excited in TM polarization. Adapted with permission from [18] © The Optical Society.

4. Conclusion

In summary, we fabricated and demonstrated different superconducting NbN nanowire detectors for polarization-independent infrared photodetection. We used a plasmonic perfect absorber circular detector structure to reach over 90% polarization-independent absorbance, due to the almost complete symmetrical plasmonic lattice in every direction and compared it to a perfect plasmonic lattice detector, reaching nearly the same high performance. Moreover, it exhibits an angle of incidence independence [18] and a tunability to desired wavelengths, by adjusting the detector geometry. The functionality of our detectors was demonstrated by exposing them to an external light source under cryogenic conditions, confirming a polarization-independent response. The perfect absorber detectors will help create smaller and hence faster detectors by coupling the photon directly in the detectors with fibers and high-NA objectives [40].

Funding. European Research Council (Complexplas); Deutsche Forschungsgemeinschaft (GRK2642); Carl-Zeiss-Stiftung; Baden-Württemberg Stiftung; Ministerium für Wissenschaft, Forschung und Kunst Baden-Württemberg (IQST); Open Access Fund University of Stuttgart; Ministry of Science and Technology, Taiwan (MOST-109-2112-M-001-043-MY3); Academia Sinica (AS-CDA-108-M08).

Acknowledgments. T. Weiss from the Institute of Physics (University of Graz) for help with the S-Matrix simulations and S. Both from the 4th Physics Institute (University of Stuttgart) for help with the S-Matrix simulations and discussions.

Disclosures. The authors declare no conflicts of interest.

Data availability. Data underlying the results presented in this paper are not publicly available at this time but may be obtained from the authors upon reasonable request.

Optical Materials EXPRESS

References

1. E. Knill, R. Laflamme, and G. J. Milburn, "A scheme for efficient quantum computation with linear optics," Nature **409**(6816), 46–52 (2001).
2. J. L. O'Brien, "Optical Quantum Computing," Science **318**(5856), 1567–1570 (2007).
3. N. Gisin, G. Ribordy, W. Tittel, and H. Zbinden, "Quantum cryptography," Rev. Mod. Phys. **74**(1), 145–195 (2002).
4. L. You, "Superconducting nanowire single-photon detectors for quantum information," Nanophotonics **9**(9), 2673–2692 (2020).
5. C. M. Natarajan, M. G. Tanner, and R. H. Hadfield, "Superconducting nanowire single-photon detectors: physics and applications," Supercond. Sci. Technol. **25**(6), 063001 (2012).
6. I. Esmaeil Zadeh, J. Chang, J. W. N. Los, S. Gyger, A. W. Elshaari, S. Steinhauer, S. N. Dorenbos, and V. Zwiller, "Superconducting nanowire single-photon detectors: A perspective on evolution, state-of-the-art, future developments, and applications," Appl. Phys. Lett. **118**(19), 190502 (2021).
7. A. J. Kerman, E. A. Dauler, J. K. W. Yang, K. M. Rosfjord, V. Anant, K. K. Berggren, G. N. Gol'tsman, and B. M. Voronov, "Constriction-limited detection efficiency of superconducting nanowire single-photon detectors," Appl. Phys. Lett. **90**(10), 101110 (2007).
8. S. Steinhauer, L. Yang, S. Gyger, T. Lettner, C. Errando-Herranz, K. D. Jöns, M. A. Baghban, K. Gallo, J. Zichi, and V. Zwiller, "NbTiN thin films for superconducting photon detectors on photonic and two-dimensional materials," Appl. Phys. Lett. **116**(17), 171101 (2020).
9. I. E. Zadeh, J. W. N. Los, R. B. M. Gourgues, V. Steinmetz, G. Bulgarini, S. M. Dobrovolskiy, V. Zwiller, and S. N. Dorenbos, "Single-photon detectors combining high efficiency, high detection rates, and ultra-high timing resolution," APL Photonics **2**(11), 111301 (2017).
10. S. Miki, T. Yamashita, H. Terai, and Z. Wang, "High performance fiber-coupled NbTiN superconducting nanowire single photon detectors with Gifford-McMahon cryocooler," Opt. Express **21**(8), 10208–10214 (2013).
11. F. Marsili, V. B. Verma, J. A. Stern, S. Harrington, A. E. Lita, T. Gerrits, I. Vayshenker, B. Baek, M. D. Shaw, R. P. Mirin, and S. W. Nam, "Detecting single infrared photons with 93% system efficiency," Nat. Photonics **7**(3), 210–214 (2013).
12. D. Rosenberg, A. J. Kerman, R. J. Molnar, and E. A. Dauler, "High-speed and high-efficiency superconducting nanowire single photon detector array," Opt. Express **21**(2), 1440–1447 (2013).
13. A. Mukhtarova, L. Redaelli, D. Hazra, H. Machhadani, S. Lequien, M. Hofheinz, J.-L. Thomassin, F. Gustavo, J. Zichi, V. Zwiller, E. Monroy, and J.-M. Gérard, "Polarization-insensitive fiber-coupled superconducting-nanowire single photon detector using a high-index dielectric capping layer," Opt. Express **26**(13), 17697–17704 (2018).
14. W. Zhang, L. You, H. Li, J. Huang, C. Lv, L. Zhang, X. Liu, J. Wu, Z. Wang, and X. Xie, "NbN superconducting nanowire single photon detector with efficiency over 90% at 1550 nm wavelength operational at compact cryocooler temperature," Sci. China Phys. Mech. Astron. **60**(12), 120314 (2017).
15. K. M. Rosfjord, J. K. W. Yang, E. A. Dauler, A. J. Kerman, V. Anant, B. M. Voronov, G. N. Gol'tsman, and K. K. Berggren, "Nanowire single-photon detector with an integrated optical cavity and anti-reflection coating," Opt. Express **14**(2), 527–534 (2006).
16. J. P. Sprengers, A. Gaggero, D. Sahin, S. Jahanmirinejad, G. Frucci, F. Mattioli, R. Leoni, J. Beetz, M. Lermer, M. Kamp, S. Höfling, R. Sanjines, and A. Fiore, "Waveguide superconducting single-photon detectors for integrated quantum photonic circuits," Appl. Phys. Lett. **99**(18), 181110 (2011).
17. A. Farag, M. Ubl, A. Konzelmann, M. Hentschel, and H. Giessen, "Utilizing niobium plasmonic perfect absorbers for tunable near- and mid-IR photodetection," Opt. Express **27**(18), 25012–25021 (2019).
18. P. Karl, S. Mennle, M. Ubl, P. Flad, J.-W. Yang, T.-Y. Peng, Y.-J. Lu, and H. Giessen, "Niobium nitride plasmonic perfect absorbers for tunable infrared superconducting nanowire photodetection," Opt. Express **29**(11), 17087–17096 (2021).
19. E. F. C. Driessen, F. R. Braakman, E. M. Reiger, S. N. Dorenbos, V. Zwiller, and M. J. A. de Dood, "Impedance model for the polarization-dependent optical absorption of superconducting single-photon detectors," Eur. Phys. J. Appl. Phys. **47**(1), 10701 (2009).
20. S. N. Dorenbos, E. M. Reiger, N. Akopian, U. Perinetti, V. Zwiller, T. Zijlstra, and T. M. Klapwijk, "Superconducting single photon detectors with minimized polarization dependence," Appl. Phys. Lett. **93**(16), 161102 (2008).
21. C. Gu, X. Chi, Y. Cheng, J. Zichi, N. Hu, X. Lan, K. Zou, S. Chen, Z. Lin, V. Zwiller, and X. Hu, "Fractal superconducting nanowire single-photon detectors with low polarization sensitivity," 2018 Conf. Lasers Electro-Optics, CLEO 2018 - Proc. 43(20), 1–4 (2018).
22. V. B. Verma, F. Marsili, S. Harrington, A. E. Lita, R. P. Mirin, and S. W. Nam, "A three-dimensional, polarization-insensitive superconducting nanowire avalanche photodetector," Appl. Phys. Lett. **101**(25), 251114 (2012).
23. J. Huang, W. J. Zhang, L. X. You, X. Y. Liu, Q. Guo, Y. Wang, L. Zhang, X. Y. Yang, H. Li, Z. Wang, and X. M. Xie, "Spiral superconducting nanowire single-photon detector with efficiency over 50% at 1550 nm wavelength," Supercond. Sci. Technol. **30**(7), 074004 (2017).
24. L. Novotny and B. Hecht, *Principles of Nano-Optics* (Cambridge University, 2006), (May).
25. X. Yin, T. Steinle, L. Huang, T. Taubner, M. Wuttig, T. Zentgraf, and H. Giessen, "Beam switching and bifocal zoom lensing using active plasmonic metasurfaces," Light Sci Appl **6**(7), e17016 (2017).
26. F. Sterl, N. Strohfeldt, S. Both, E. Herkert, T. Weiss, and H. Giessen, "Design Principles for Sensitivity Optimization in Plasmonic Hydrogen Sensors," ACS Sens. **5**(4), 917–927 (2020).

Optical Materials EXPRESS

27. M. Tanzid, A. Ahmadivand, R. Zhang, B. Cerjan, A. Sobhani, S. Yazdi, P. Nordlander, and N. J. Halas, "Combining Plasmonic Hot Carrier Generation with Free Carrier Absorption for High-Performance Near-Infrared Silicon-Based Photodetection," ACS Photonics **5**(9), 3472–3477 (2018).
28. Q. Sun, C. Zhang, W. Shao, and X. Li, "Photodetection by Hot Electrons or Hot Holes: A Comparable Study on Physics and Performances," ACS Omega **4**(3), 6020–6027 (2019).
29. W. Wang, C. Zhang, K. Qiu, G. Li, A. Zhai, Y. Hao, X. Li, and Y. Cui, "Enhancing Hot-Electron Photodetection of a TiO2/Au Schottky Junction by Employing a Hybrid Plasmonic Nanostructure," Materials **15**(8), 2737 (2022).
30. A. Tittl, A. K. U. Michel, M. Schäferling, X. Yin, B. Gholipour, L. Cui, M. Wuttig, T. Taubner, F. Neubrech, and H. Giessen, "A Switchable Mid-Infrared Plasmonic Perfect Absorber with Multispectral Thermal Imaging Capability," Adv. Mater. **27**(31), 4597–4603 (2015).
31. N. I. Landy, S. Sajuyigbe, J. J. Mock, D. R. Smith, and W. J. Padilla, "Perfect Metamaterial Absorber," Phys. Rev. Lett. **100**(20), 207402 (2008).
32. N. Liu, M. Mesch, T. Weiss, M. Hentschel, and H. Giessen, "Infrared perfect absorber and its application as plasmonic sensor," Nano Lett. **10**(7), 2342–2348 (2010).
33. R. Walter, A. Tittl, A. Berrier, F. Sterl, T. Weiss, and H. Giessen, "Large-area low-cost tunable plasmonic perfect absorber in the near infrared by colloidal etching lithography," Adv. Opt. Mater. **3**(3), 398–403 (2015).
34. A. Tittl, P. Mai, R. Taubert, D. Dregely, N. Liu, and H. Giessen, "Palladium-based plasmonic perfect absorber in the visible wavelength range and its application to hydrogen sensing," Nano Lett. **11**(10), 4366–4369 (2011).
35. P. Karl, M. Ubl, M. Hentschel, P. Flad, Z. Y. Chiao, J. W. Yang, Y. J. Lu, and H. Giessen, "Optical properties of niobium nitride plasmonic nanoantennas for the near- and mid-infrared spectral range," Opt. Mater. Express **10**(10), 2597–2606 (2020).
36. Y. J. Lu, R. Sokhoyan, W. H. Cheng, G. K. Shirmanesh, A. R. Davoyan, R. A. Pala, K. Thyagarajan, and H. A. Atwater, "Dynamically controlled Purcell enhancement of visible spontaneous emission in a gated plasmonic heterostructure," Nat. Commun. **8**(1), 1631 (2017).
37. T. Weiss, G. Granet, N. A. Gippius, S. G. Tikhodeev, and H. Giessen, "Matched coordinates and adaptive spatial resolution in the Fourier modal method," Opt. Express **17**(10), 8051–8061 (2009).
38. T. Weiss, N. A. Gippius, S. G. Tikhodeev, G. Granet, and H. Giessen, "Efficient calculation of the optical properties of stacked metamaterials with a Fourier modal method," J. Opt. A: Pure Appl. Opt. **11**(11), 114019 (2009).
39. L. Novotny, "Effective Wavelength Scaling for Optical Antennas," Phys. Rev. Lett. **98**(26), 266802 (2007).
40. M. Sartison, K. Weber, S. Thiele, L. Bremer, S. Fischbach, T. Herzog, S. Kolatschek, M. Jetter, S. Reitzenstein, A. Herkommer, P. Michler, S. L. Portalupi, and H. Giessen, "3D printed micro-optics for quantum technology: Optimised coupling of single quantum dot emission into a single-mode fibre," gxjzz **2**(2), 103 (2021).
41. L. Bremer, K. Weber, S. Fischbach, S. Thiele, M. Schmidt, A. Kaganskiy, S. Rodt, A. Herkommer, M. Sartison, S. L. Portalupi, P. Michler, H. Giessen, and S. Reitzenstein, "Quantum dot single-photon emission coupled into single-mode fibers with 3D printed micro-objectives," APL Photonics **5**(10), 106101 (2020).
42. F. Flassig, R. Flaschmann, T. Kainz, S. Ernst, S. Strohauer, C. Schmid, L. Zugliani, K. Müller, and J. J. Finley, "Automated, deep reactive ion etching free fiber coupling to nanophotonic devices," Proc. SPIE **12009**, 120090F (2022).
43. X. Yang, L. You, L. Zhang, C. Lv, H. Li, X. Liu, H. Zhou, and Z. Wang, "Comparison of superconducting nanowire single-photon detectors made of NbTiN and NbN thin films," IEEE Trans. Appl. Supercond. **28**(1), 1–6 (2018).
44. S. Miki, M. Fujiwara, M. Sasaki, B. Baek, A. J. Miller, R. H. Hadfield, S. W. Nam, and Z. Wang, "Large sensitive-area NbN nanowire superconducting single-photon detectors fabricated on single-crystal MgO substrates," Appl. Phys. Lett. **92**(6), 061116–2009 (2008).
45. L. You, X. Yang, Y. He, W. Zhang, D. Liu, W. Zhang, L. Zhang, L. Zhang, X. Liu, S. Chen, Z. Wang, and X. Xie, "Jitter analysis of a superconducting nanowire single photon detector," AIP Adv. **3**(7), 072135 (2013).